energies

MDPI

Article

Parametric Analysis of Design Parameter Effects on the Performance of a Solar Desiccant Evaporative Cooling System in Brisbane, Australia

Yunlong Ma [1], Suvash C. Saha [1,*], Wendy Miller [1] and Lisa Guan [2]

[1] School of Chemistry Physics and Mechanical Engineering, Queensland University of Technology (QUT), 2 George Street, Brisbane, QLD 4000, Australia; yunlong.ma@hdr.qut.edu.au (Y.M.); w2.miller@qut.edu.au (W.M.)

[2] Faculty of Design, Architecture & Building, University of Technology Sydney, PO Box 123, Broadway, Sydney, NSW 2007, Australia; lishanlisa.guan@uts.edu.au

* Correspondence: suvash.saha@qut.edu.au; Tel.: +61-7-3138-1413

Received: 25 May 2017; Accepted: 23 June 2017; Published: 25 June 2017

Abstract: Solar desiccant cooling is widely considered as an attractive replacement for conventional vapor compression air conditioning systems because of its environmental friendliness and energy efficiency advantages. The system performance of solar desiccant cooling strongly depends on the input parameters associated with the system components, such as the solar collector, storage tank and backup heater, etc. In order to understand the implications of different design parameters on the system performance, this study has conducted a parametric analysis on the solar collector area, storage tank volume, and backup heater capacity of a solid solar desiccant cooling system for an office building in Brisbane, Australia climate. In addition, a parametric analysis on the outdoor air humidity ratio control set-point which triggers the operation of the desiccant wheel has also been investigated. The simulation results have shown that either increasing the storage tank volume or increasing solar collector area would result in both increased solar fraction (*SF*) and system coefficient of performance (*COP*), while at the same time reduce the backup heater energy consumption. However, the storage tank volume is more sensitive to the system performance than the collector area. From the economic aspect, a storage capacity of 30 m^3/576 m^2 has the lowest life cycle cost (*LCC*) of $405,954 for the solar subsystem. In addition, 100 kW backup heater capacity is preferable for the satisfaction of the design regeneration heating coil hot water inlet temperature set-point with relatively low backup heater energy consumption. Moreover, an outdoor air humidity ratio control set-point of 0.008 kgWater/kgDryAir is more reasonable, as it could both guarantee the indoor design conditions and achieve low backup heater energy consumption.

Keywords: parametric analysis; design parameters; desiccant cooling; evaporative cooling; solar energy; building simulation; EnergyPlus

1. Introduction

Solar desiccant cooling technology has been widely investigated and applied all over the world during the past years. It has been found to be environmentally friendly, and in some circumstances economically beneficial, as it is able to improve indoor air quality while at the same time reducing energy consumption [1,2]. The basic solar desiccant cooling system generally combines the desiccant process with evaporative cooling. A typical solar desiccant evaporative cooling (SDEC) system is mainly comprised of: (1) a solar subsystem which consists of solar collectors, a storage tank and a backup heater; (2) a desiccant subsystem which includes a desiccant wheel, desiccant materials (usually silica gel), a regeneration heating coil, and a sensible air-to-air heat exchanger; and (3) evaporative coolers. The schematic diagram of a typical SDEC system is illustrated in Figure 1 [3].

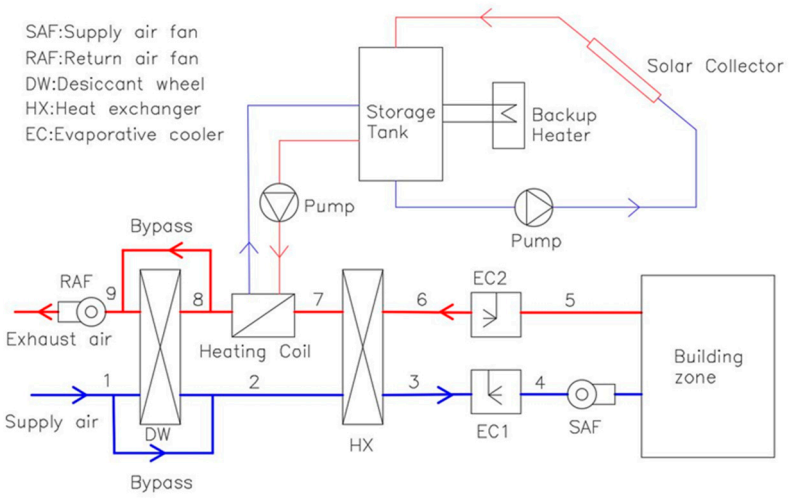

Figure 1. Schematic diagram of the basic solar desiccant evaporative cooling system [3].

The SDEC system treats the sensible load and latent load of the supply air separately. The working principle of the solar desiccant cooling system is that the desiccant material in the desiccant wheel first dries and heats the outside air (1–2), then the dehumidified process air is cooled to near ambient temperature through a sensible air-to-air rotary heat exchanger (2–3). The process air is further cooled by the evaporative cooler (3–4) and is eventually sent to the conditioned space. In the regeneration air stream, the return air is cooled by a second evaporative cooler (5–6) in order to increase the heat exchanger's efficiency. It is then heated to the regeneration temperature by the regeneration air heater (7–8). The continuous air dehumidification process saturates the desiccant material which must be regenerated in order to continue to perform its function. Thus, solar thermal energy is supplied to the regeneration heating coil for regeneration purposes. A backup heater is usually included whenever solar energy is insufficient.

Currently many research articles have examined the performance of the solar desiccant cooling system in the world. Baniyounes et al. [1] conducted the study of a solar desiccant cooling for an institutional building in Australian subtropical climate Rockhampton using TRNSYS 16 (software developed at the University of Wisconsin, Madison, SD, USA). They demonstrated that the system would achieve an annual coefficient of performance (*COP*) of 0.7, a 22% solar fraction (*SF*), 4.4 tonnes of greenhouse gas (GHG) emissions reduction, and 22 years payback by installing 10 m^2 solar collectors and 0.4 m^3 storage tank. Angrisani et al. [2] assessed the energy, environmental, and economic performances of a solar desiccant-based air handling unit (AHU) with three types of collectors: solar air collector, flat plate collector, and evacuated tube collector. They found that energy and environmental benefits increased with the solar collector surface, but the thermo-economic performance was not in proportion to the solar collector surface. The best solution for achieving the economic feasibility of the solar desiccant cooling system was the installation of 16 m^2 evacuated tube collectors, which allowed 50.2% primary energy savings and 49.8% CO_2 emissions reduction compared to the referenced conventional system, with about 20 years payback period. Rafique et al. [4] conducted a theoretical analysis of desiccant-based evaporative cooling systems for five cities in Saudi Arabia. They found that the system thermal *COP* ranged from 0.275 to 0.476 based on different locations. They also concluded that an increase of 15% in evaporative cooler effectiveness resulted in about 15 to 25% increase in the system thermal *COP*. Furthermore, a decrease in system *COP* would be caused by an increase in regeneration temperature and process/regeneration air flow ratio. In addition, the desiccant wheel dehumidifying efficiency increased with the increase of the ambient air humidity ratio. Angrisani et al. [5] again investigated three alternative configurations of an innovative solar-assisted hybrid desiccant-based AHU through TRNSYS 16 simulation: (1) heat recovery from the chiller heat rejection for pre-heating the regeneration air; (2) pre-heating of regeneration air with

the warmer regeneration air exiting the desiccant wheel; and (3) pre-cooling of the process air before entering the desiccant wheel. By considering different collector types, surface areas and tilt angles, they indicated that the desiccant-based AHU with evacuated tube collectors could achieve 15 to 24% primary energy conservation and 14 to 22% CO_2 emissions reduction compared to conventional cooling systems. If the optimal configurations in terms of the solar thermal energy utilisation, surface areas, and tilt angles were adopted, the evacuated tube collectors could ensure 73% primary energy savings and 71% avoided equivalent CO_2 emissions with only 6 years payback period. Li et al. [6] conducted a case study of a two-stage solar desiccant air conditioning system using evacuated tube air collectors in China. They found that the average thermal *COP* could be 0.97 in cooling and 0.45 in heating. Ge et al. [7] compared the performance of a two-stage solar rotary desiccant cooling system with a conventional vapour compression system under Berlin and Shanghai climates. They indicated that the SDEC system was able to meet the cooling demand and produce comfortable supply air in both cities with less energy consumption, and the payback period was 4.7 years for Berlin and 7.2 years for Shanghai, respectively.

There are also a number of recent research studies that have been investigated to evaluate the impacts of various system components design parameters on the solar desiccant cooling system performance in different climates. Goldsworthy and White [8] conducted the numerical optimisation of a solar desiccant cooling system for a certain climatic zone in Australia. They found that for 70 °C regeneration temperature, a supply/regeneration flow ratio of 0.67 and an indirect evaporative cooler secondary/primary flow ratio of 0.3 gave the best system performance with the electric *COP* above 20 for this particular location. It should be noted that the electric *COP* of the SDEC system reported in the study is much larger than the thermal *COP* (ranges from 0.275 to 0.97) discussed above. This is because of the different definitions and calculation formulas between the thermal *COP* and electric *COP*. The thermal *COP* is defined as the ratio between the system cooling effect to the external heat delivered to the regeneration air heater; while the electric *COP* is calculated as the system cooling effect to the total system electricity consumption including fans, pumps, and auxiliary heater, etc. [9]. The definition and formula expression of the electric *COP* is quite similar to the energy efficient ratio (EER), which also takes into consideration of the consumption of electrical-consumed auxiliary devices. White et al. [10] assessed the performance of a solar desiccant cooling system without thermal backup for office spaces located in Melbourne, Sydney, and Darwin. They concluded that increasing the indirect evaporative effectiveness, supply air flow rate, and solar collector areas would apparently result in reduced frequency of high indoor temperature events in Melbourne and Sydney, but this impact was not evident in Darwin due to high outdoor air temperature and humidity ratio in Darwin. Parmar and Hindoliya [11] conducted a comparable study of a SDEC system for various Indian climates. They concluded that a regeneration/process air ratio (R/P ratio) of 0.55 led to the maximum thermal *COP* of 4.98 in warm and humid climates such as Mumbai with less regeneration power and that the increase of the R/P ratio would result in decreased system *COP* and increased regeneration heat requirement. It should also be noticed that according to [9], the thermal *COP* of a solar desiccant cooling system strongly depends on the conditions of ambient air, supply air, and return air, and the value usually ranges from 0.5 to 1.0. In this study however, the high thermal *COP* value of 4.98 is because that the system thermal *COP* is highly sensitive to the R/P ratio. In addition, the warm and humid outside air conditions in Mumbai make the solar desiccant cooling system more feasible and advantageous. Zahra et al. [12] presented an optimisation study of the required solar air collector areas for a solar desiccant cooling system in Iran by considering the desiccant wheel parameters and operating conditions. They found that the solar air collector surface would be decreased by increasing the collector inlet air dry-bulb temperature, inlet air humidity ratio, and solar irradiance; and it would be increased by increasing the regeneration air temperature. Panaras et al. [13] investigated the influential design parameters for the solar desiccant cooling system performance and they indicated that the air flow rate, regeneration temperature, operation cycle, and outdoor conditions have significant impacts on the solar desiccant cooling system performance.

Rafique et al. [14] conducted a parametric analysis of a rotary liquid desiccant cooling system under various operating and climatic conditions. The parameters considered included evaporative cooler effectiveness, outside air temperature and humidity ratio, ratio of regeneration air to process air mass flow rate, and regeneration temperature. It was found that the increase of the evaporative cooler effectiveness would significantly improve the system performance. In addition, decreasing the regeneration/process air mass flow rate ratio and regeneration temperature was beneficial for the performance of the system. Apart from the solar desiccant cooling system parameters analysis, Giulio et al. [15] conducted a dynamic multi-level simulation using Matlab/Simulink for a solar adsorption cooling system to identify the correlations among different input variables and the climatic data. By performing the Fourier analysis, they concluded that the most important parameters influencing the system *COP*, in order of importance, were ambient air temperature, condensation power of the adsorption chiller, chiller cooling effect, and heating power used by the chiller. They also found that the thermal power delivered to the hot storage unit was strongly correlated with, in order of priority, the adsorbent material temperature, condensation temperature, ambient temperature, and the heating power used by the chiller.

From the literature review, it appears that previous research has indicated some implications of the system components design parameters on the system performance, such as maximising the system *COP*, minimising the solar collector areas, and reducing the frequency of high indoor temperature events. However, little research has been conducted about the impacts of different system components design parameters on the energy performance of the solar desiccant cooling system. In addition, there is little research about the parametric analysis of the SDEC system from the whole system performance point of view. There is also little research studies to evaluate the impacts of solar collector areas, storage tank volumes, backup heater capacities, and outdoor air humidity ratio control on the SDEC system performance in subtropical climate in Australia. Therefore, the purpose of this paper is to identify the impacts of the system components design parameters on the SDEC system technical and energy performances in Australia, in terms of solar collector area, storage tank volume, and backup heater capacity. In addition, an energy management system (EMS) control on the outdoor air humidity ratio set-point which triggers the operation of the desiccant wheel has also been evaluated. This study aims at establishing fundamental understanding of the influential design parameters that impact the SDEC system performance under Australian climate and providing implications for the whole system optimisation.

2. Methods

2.1. Building Characteristics

The parametric investigation of different design parameters on the proposed SDEC system performance is based on computer simulation using EnergyPlus. The building to be modelled is a three-storey, 5-zone per floor, rectangular office building with a carpark, as shown in Figure 2. The total conditioned window-to-wall ratio (WWR) is 0.4, with the North and South facades of 36.5 m $\times$ 1.35 m, and the East and West facades of 18.3 m $\times$ 0.54 m for each floor. The selection of this building model is because it is recommended by the Australian building codes board (ABCB) to be a representative medium-sized commercial building in the central business district in Australia for energy modelling [16], and it is widely studied in other projects [16–21]. The climatic location is Brisbane, Australia.

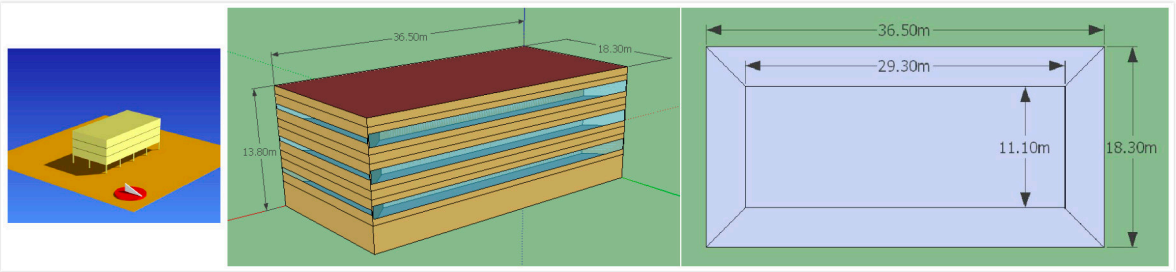

Figure 2. Building model geometry and zone division.

The building's physical properties, internal load density and operation schedules are shown in Tables 1 and 2 respectively.

Table 1. Building model physical properties [16].

Building Feature	Value
Number of storeys	3
Footprint dimensions	36.5 m × 18.3 m
Gross conditioned floor area	2003.85 m^2
Aspect ratio	2:1
Floor-to-ceiling height	2.7 m
Plenum wall height	0.9 m
Car park height	3 m
Building total height	13.8 m
Orientation	Long axis East-West
Number of zones per floor	5
Roof	Metal deck, air gap, foil, roof space, R2.0 batts, 13 mm acoustic tiles (U = 0.277 W/m^2K)
Floor	175 mm concrete slab with carpet (U = 1.32 W/m^2K)
Exterior wall	200 mm heavy weight concrete, R1.5 batts, 10 mm plasterboard (U = 0.554 W/m^2K)
Window	Single 6 mm clear glass, (U = 5.89 W/m^2K)
Window-to-wall ratio	0.4
Floor-to-ceiling height	2.7 m
Plenum wall height	0.9 m

Table 2. Modelling assumptions of internal load density and operational schedules [22].

Modelling Assumptions	Value
Lighting power density	15 W/m^2
Equipment load density	15 W/m^2
Occupant density	10 m^2/person
Lighting schedule	91.5 h/week
Equipment schedule	97.45 h/week
Occupancy schedule	53.75 h/week
HVAC (heating, ventilation, and air conditioning) operation schedule	60 h/week, 06:00–18:00, Monday to Friday
Infiltration rate	1 ACH (air change per hour), no infiltration during HVAC operation
Outside air rate	10 L/s per person
HVAC set-points	24 ± 1 °C, 50% relative humidity for cooling with setback temperature of 38 °C; 20 ± 1 °C for heating with setback temperature of 12 °C

The infiltration rate is set as 1 ACH outside the HVAC operation and it assumes no infiltration when the HVAC is on, which is referenced from [19]. The building code of Australia volume one of the national construction code 2016 [23] specifies that energy modelling infiltration rate is defined as 1 ACH for perimeter zones only during HVAC operation, and 1.5 ACH for whole building outside HVAC operation, which is also adopted by [16]. The infiltration rate adopted in this study is a little tighter than the Australian code specified. Generally the less air leakage the better the building energy

performance as is concluded by Egan [24]. However, the changes in infiltration rate in this study would not dramatically influence the energy consumption results for a building that is located in hot summer warm winter climates with fixed windows, as is concluded by Feng et al. [25].

2.2. System Components Modelling

2.2.1. Solar Thermal Collector

In this study, the flat plate solar thermal collector is used for the simulation. The reason for the selection of this type of solar thermal collector is because according to Henning [26], flat plate solar thermal collectors are the most commonly used solar thermal collector type, dominating the market with about 90% market penetration around the world. In addition, according to international energy agency (IEA) solar heating and cooling program task 48 [27], the flat plate solar thermal collector is able to produce as high as 100 °C hot water, which is enough for driving the solar desiccant cooling system. Another important reason for the selection of the flat plate solar thermal collector is that in EnergyPlus, only the SolarCollector:FlatPlate:Water object is available to model solar thermal collectors, which can represent the performance of single glazed, unglazed or evacuated tube collectors. Finally, the flat plate solar thermal collector is much more cost effective than the evacuated tube solar thermal collector for low temperature applications such solar cooling and heating [28]. The governing equations for the modelling of the solar thermal collector are expressed as [29]:

$$Q_{Solar} = \eta_{Solar} \times A_c \times I \tag{1}$$

$$\eta_{Solar} = c_0 + c_1 \times \frac{T_{in} - T_a}{I} + c_2 \times \frac{(T_{in} - T_a)^2}{I} \tag{2}$$

where η_{Solar} is the solar thermal collector overall efficiency; A_c is the gross area of the solar thermal collector in m^2; I is the total incident solar radiation in W/m^2; T_{in} is the collector inlet temperature of the working fluid in °C; T_a is the ambient air temperature in °C; c_0 is the collector optical efficiency; c_1 and c_2 are the collector heat loss coefficients.

2.2.2. Desiccant Wheel

In EnergyPlus, the desiccant wheel is modelled as a balanced flow desiccant heat exchanger which deals with both sensible and latent heat transfer between the process and regeneration air streams. It assumes the same air volume flow rate and face velocity through the regeneration and process air stream sides and no heat or humidity losses to the environment. The governing equations for the modelling of the desiccant wheel are [29]:

$$RTO = B_1 + B_2 \times RWI + B_3 \times RTI + B_4 \times \left(\frac{RWI}{RTI}\right) + B_5 \times PWI + B_6 \times PTI + B_7 \times \left(\frac{PWI}{PTI}\right) + B_8 \times RFV \tag{3}$$

$$RWO = C_1 + C_2 \times RWI + C_3 \times RTI + C_4 \times \left(\frac{RWI}{RTI}\right) + C_5 \times PWI + C_6 \times PTI + C_7 \times \left(\frac{PWI}{PTI}\right) + C_8 \times RFV \tag{4}$$

where RTO is regeneration outlet air (point 9 in Figure 1) dry bulb temperature in °C; RWI is regeneration inlet air (point 8 in Figure 1) humidity ratio in kgWater/kgDryAir; RTI is regeneration inlet air dry bulb temperature in °C; PWI is process inlet air (point 1 in Figure 1) humidity ratio in kgWater/kgDryAir; PTI is process inlet air dry bulb temperature in °C; RFV is regeneration (and process) face velocity in m/s; B_n is temperature equation coefficient; RWO is regeneration outlet air humidity ratio in kgWater/kgDryAir; and C_n is humidity ratio equation coefficient.

Once the regeneration outlet air conditions are determined as described above, the dry bulb temperature and humidity differences across the regeneration side of the desiccant wheel can be

calculated. Since the desiccant wheel is based on the assumptions of zero heat and humidity losses to the environment, the following equations can be obtained:

$$t_1 - t_2 = t_9 - t_8 \tag{5}$$

$$w_1 - w_2 = w_9 - w_8 \tag{6}$$

The coefficients of B_n and C_n are shown in Table 3 below from the manufacturer's data (EDC-3550-200) [30]. The selection of this desiccant wheel model is because it can meet with the requirement of the system supply air flow rate (69,753 m^3/h nominal process air volume), and it has good dehumidifying effect which is able to dehumidify the outdoor air humidity below 0.005 kgWater/kgDryAir [30]. Therefore, a humidity ratio control set-point of 0.005 kgWater/kgDryAir is applied on the desiccant wheel process air outlet node (point 2 in Figure 1) for dehumidifying control purposes [31].

Table 3. Coefficients for desiccant wheel temperature and humidity ratio equations.

B1	B2	B3	B4	B5	B6	B7	B8
−27.18302	−184.97	1.00051	11603.3	−50.755	−0.0168467	58.2213	0.598863
C1	**C2**	**C3**	**C4**	**C5**	**C6**	**C7**	**C8**
0.01213878	1.09689	−0.000026	−6.3389	0.00938196	0.0000521186	0.0670354	−0.0001608

2.2.3. Sensible Air-to-Air Heat Exchanger

The sensible air-to-air heat exchanger presents air streams of equal flow rate and no heat losses to the environment. It is modelled based on the following equations [29]:

$$\varepsilon_{HX} = \frac{t_2 - t_3}{t_2 - t_6} \tag{7}$$

$$t_2 - t_3 = t_7 - t_6 \tag{8}$$

where ε_{HX} is heat exchanger effectiveness; t_2 is heat exchanger process air inlet (point 2 in Figure 1) dry bulb temperature in °C; t_3 is heat exchanger process air outlet (point 3 in Figure 1) dry bulb temperature in °C; t_6 is heat exchanger regeneration air inlet (point 6 in Figure 1) dry bulb temperature in °C; and t_7 is heat exchanger regeneration air outlet (point 7 in Figure 1) dry bulb temperature in °C.

2.2.4. Evaporative Cooler

The direct evaporative cooler is modelled using the following equation [29]. It assumes a constant effectiveness model and the wet bulb temperature remains constant between the inlet and outlet of the direct evaporative cooler:

$$T_{db,out} = T_{db,in} - \varepsilon(T_{db,in} - T_{wb,in}) \tag{9}$$

where $T_{db,out}$ is the dry bulb temperature of the air leaving the cooler (point 4 and 6 in Figure 1) in °C; $T_{db,in}$ is the dry bulb temperature of the air entering the cooler (point 3 and 5 in Figure 1) in °C; $T_{wb,in}$ is the wet bulb temperature of the air entering the cooler in °C; and ε is the cooler effectiveness.

2.3. Performance Indicators

2.3.1. Solar Fraction

Solar fraction is an important technical indicator to assess the feasibility of the solar cooling systems: the higher the *SF*, the greater the contribution of solar energy to the system. *SF* is the ratio of solar energy contribution to the total energy input for driving the solar cooling system. A backup

heater is usually used to deliver the required thermal energy when solar energy is insufficient to drive the cooling system. Therefore, the solar fraction can be defined in the following equation:

$$SF = \frac{E_{Solar}}{E_{in}} = \frac{E_{Solar}}{E_{hvac} + E_{Solar}} \tag{10}$$

where E_{Solar} refers to the useful solar thermal energy input in GJ (gigajoule); E_{in} is the total energy input requirement for driving the solar cooling system in GJ; and E_{hvac} is the energy consumption of all the electrical components in the system in GJ, including fans, pumps, backup heater, evaporative coolers, and desiccant wheel motor.

2.3.2. System Coefficient of Performance

In this study, electric *COP* is used as the technical performance indicator and is defined as the ratio of the system total cooling effect to the total HVAC electricity consumption from the city electricity grid, which can be expressed in Equation (11) below:

$$COP = \frac{Q_C}{W_{hvac}} = \frac{m_o \times (h_o - h_s)}{W_{hvac}} \tag{11}$$

where m_o is the outside air mass flow rate in kg/s; h_o is the enthalpy of outside air in kJ/kg; and h_s is the enthalpy of supply air after the evaporative cooler 1 (point 4 in Figure 1) in kJ/kg.

2.3.3. Annual Backup Heater Electricity Consumption

Electricity energy consumption is one of the most important energy performance indicators to evaluate the SDEC system performance. Only the backup heater energy consumption is counted in this research because the electricity consumption of pumps, evaporative coolers, and desiccant wheel motor can be neglected compared with the system total energy consumption [1], and the inclusion of fan power consumption would not dramatically change the results [10]. In other words, the variation of the solar collector area, storage tank volume, backup heater capacity, and humidity ratio control set-point would not significantly influence the electricity energy consumption of fans, pumps, evaporative coolers and desiccant wheel motor. The backup heater electricity consumption is calculated as [29]:

$$E_{Aux} = \frac{mC_w(T_{set} - T_{in}) + U_A(\overline{T} - T_a)}{\eta} \tag{12}$$

where m is the water mass flow rate in kg/s; C_w is water specific heat in kJ/(kg·°C); η is the backup heater efficiency; T_{set} is the hot water set-point temperature in the backup heater in °C; T_{in} is the water inlet temperature in °C; U_A is the overall heat loss coefficient between the backup heater and the environment during operation; $\overline{T}$ is $(T_{set} + T_{in})/2$ and T_a is the ambient environment temperature in °C.

2.4. General System Input Parameters and Validation

The general system input parameters used for the simulation are summarised in Table 4 below.

Generally the electricity backup heater efficiency is 1 during operation and thus no heat loss to the environment [32]. The solar collector data is chosen from EnergyPlus datasets. The selection of the regenerative hot water loop flow rate is based on the assumption of 30 °C temperature differences between the regeneration heating coil inlet and outlet. The simulation parameters for the desiccant wheel and sensible air-to-air heat exchanger are from manufacturers' data [30,33].

Table 4. General system input parameters in EnergyPlus simulation.

Parameters	Value	Parameters	Value
Backup heater	-	*Heat exchanger (HX)*	-
Backup heater fuel type	Electricity	HX type	Flat Plate
Backup heater efficiency	1	Nominal air flow rate (m^3/s)	19.4
Solar thermal collector (Solahart Industries Bt)	-	Ratio of supply to secondary h·A values	1
Collector optical efficiency c_0	0.753	Nominal electric power (W)	0
Collector heat loss coefficient c_1 ($W/m^2 \cdot K$)	−5.2917	Nominal supply air inlet temperature (°C)	54
Collector heat loss coefficient c_2 ($W/m^2 \cdot K^2$)	0.00638	Nominal supply air outlet temperature (°C)	32.4
Collector fluid flow rate per unit area ($kg/s \cdot m^2$)	0.019	Nominal secondary air inlet temperature (°C)	20
Collector tilt	25°	*Direct evaporative cooler*	-
Solar collector type	Flat Plate	Coil maximum efficiency	0.9
Regenerative hot water loop	-	Recirculating water pump power (W)	50
Hot water design set-point (°C)	75	*Regeneration heating coil*	-
Hot water loop flow rate (kg/s)	2.4	Regeneration air heater capacity (kW)	300
Desiccant wheel (DW)	-	Rated ratio for air and water convection	0.5
Nominal air flow rate (m^3/s)	19.4	Supply air temperature set-point (°C)	14
Nominal electric power (W)	186	*Supply & regeneration air fan*	-
Nominal air face velocity (m/s)	4	Fan delta pressure (Pa)	500
Minimum regeneration temperature (°C)	50	Fan total efficiency	0.7

For the building model and system validation, experimental measured data is not available as this is an archetypal building and no existing SDEC system is in operation with this building model. Therefore, the building indoor design conditions are used for the validation. Figure 3 shows the monthly building cooling and heating load. Figure 4 below shows the simulation results of the monthly building indoor temperature and relative humidity.

Figure 3 demonstrates that in Brisbane, for the Building Form B, cooling is dominant and is required all year round. The maximum cooling load occurs in March with 31.3 MWh, while the minimum cooling load happens in July with about 19 MWh. For the heating load profile, the heating load is only required in June, July and August with about 6 kWh, 10.44 kWh and 8.45 kWh respectively.

From Figure 4 it can be seen that the SDEC system can meet the indoor design set-point conditions of 24 ± 1 °C and 50% relative humidity for occupied cooling, and the monthly averaged building indoor temperature results coincide with the monthly building loads, indicating that the building model and the SDEC system are constructed correctly.

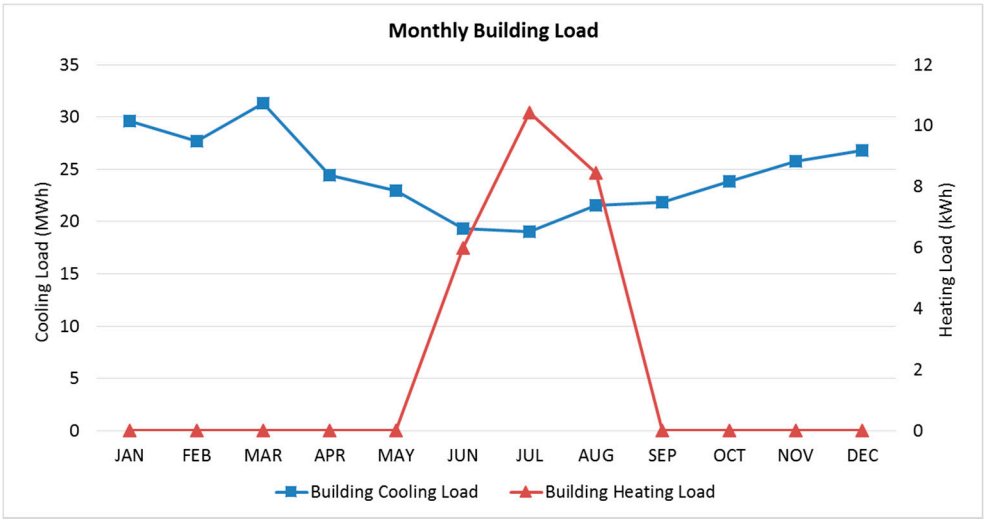

Figure 3. Monthly building cooling and heating load.

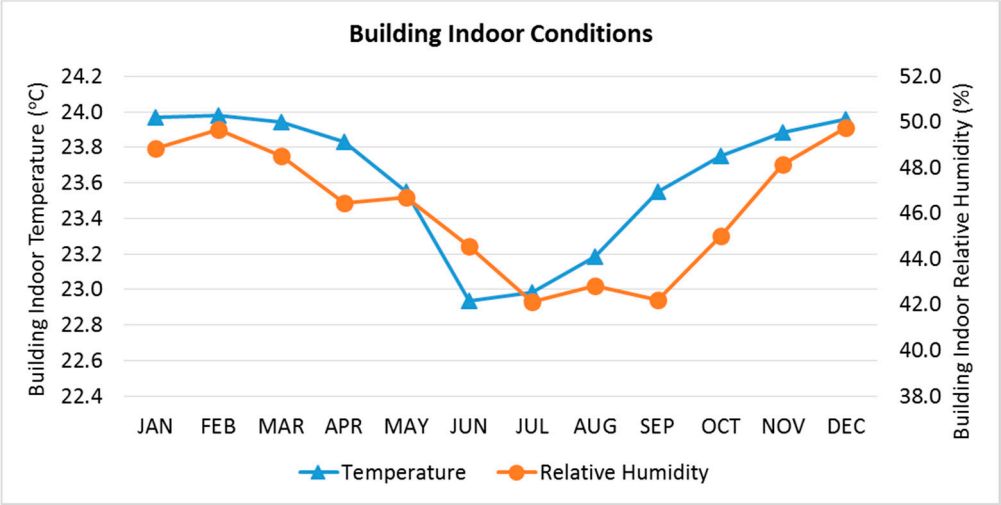

Figure 4. Monthly averaged building indoor temperature and relative humidity.

A psychrometric chart of the SDEC system air processing procedure under the summer design condition is also demonstrated in Figure 5 below, which clearly illustrates the temperature and humidity ratio conditions of the air in each state point specified in Figure 1. The blue line indicates the process air stream and the red line indicates the regeneration air stream. It shows that under the summer design cooling condition, the SDEC system could provide the designed supply air temperature of 14 °C and keep the indoor conditions of 24 °C and 50% relative humidity. This could also provide some reliability and confidence for the building and system model validation.

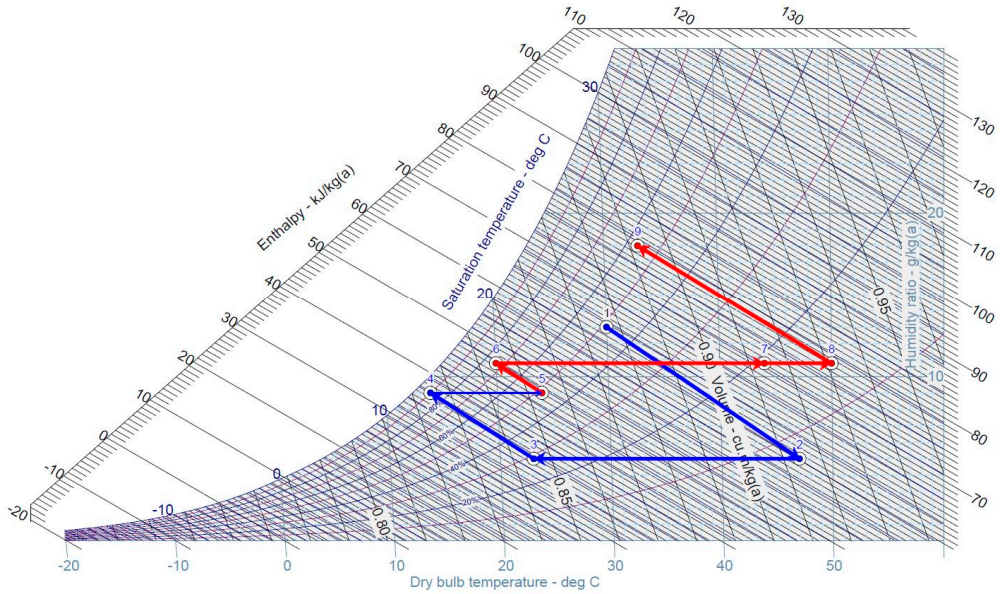

Figure 5. Psychrometric chart of the SDEC system air processing stages.

3. Results and Discussion

3.1. The Impacts of Storage Tank Volume

According to [4], the recommended storage capacity for a solar cooling system is 50–100 L/m^2 of the collector area. This can act as an indication and guidance to choose the values for the storage tank volume sensitivity analysis. The storage tank volume sensitivity examination simulations are based on

a fixed collector area of 576 m^2 and backup heater capacity of 100 kW. In order to justify the impacts of the storage tank volume on the SDEC system performance, five values are investigated: 10, 20, 30, 40 and 50 m^3. The placement of the storage tank is not a key issue in this research; therefore, structural loading is not taken into the consideration. It could be assumed that the storage tank could be located in the plant room, basement, on the ground outside the building, or could be split into several small tanks. Figures 6 and 7 below show the impacts of changing storage tank volume on the system solar fraction and *COP*, respectively.

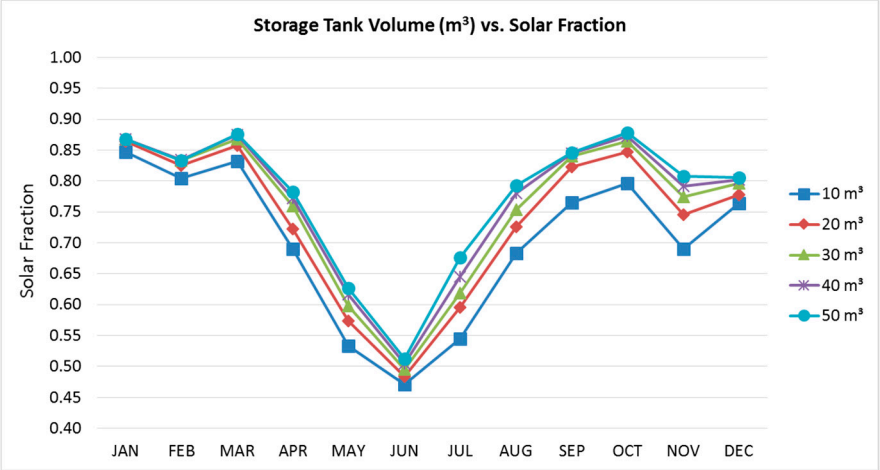

Figure 6. The impact of storage tank volume on solar fraction.

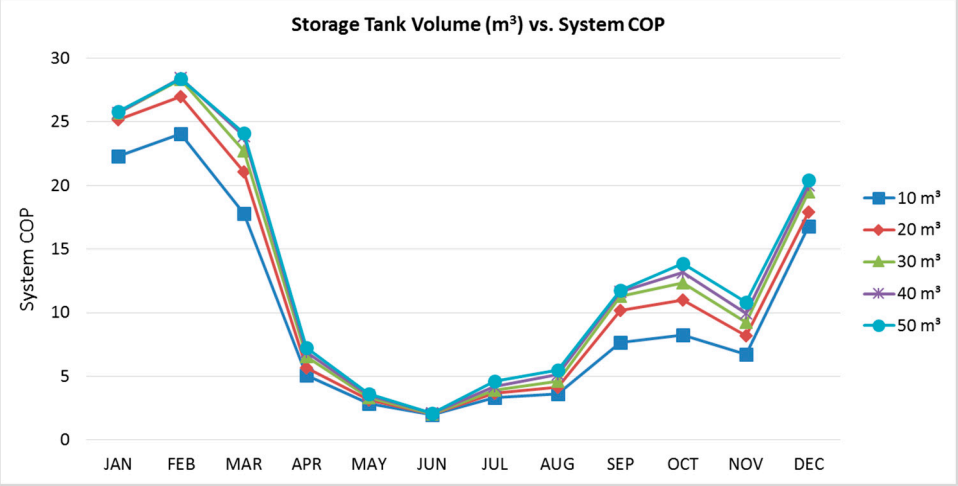

Figure 7. The impact of storage tank volume on system COP.

As shown in Figure 6, it can be seen that the system *SF* increases with the increase of the hot water storage tank volume. The annual averaged *SF* achieves 0.7 when the storage tank volume is 10 m^3 and goes up to 0.78 when a 50 m^3 storage tank is installed. However, with the increase of the storage tank volume, the growth of the *SF* becomes less obvious. In addition, the *SF* increment in April to November is much larger than in other months except June. This is because in these months, the solar thermal energy availability ratio has increased dramatically with the enhancement of the storage tank volume. Generally the monthly *SF* in summer seasons is higher than in winter periods, which is also due to relatively low HVAC system input energy consumption and high solar energy utilisation (solar energy applied to the regenerative heating coil for regeneration, but not the solar energy gathered by

the collectors at that period). Therefore, the larger the storage tank volume, the more the solar energy utilisation rate.

Figure 7 indicates that the system electric *COP* increases with the enhancement of the storage tank volume. The increment is more apparent in summer months from January to March, and from September to December. This is because in these months, the increase of the storage tank volume would lead to more available solar energy utilisation and thus less backup heater energy consumption. The maximum *COP* happens in February with as high as about 24.1 to 28.5 for different tank volumes. These results are also coincident with the results studied in [8] by Goldsworthy and White that an electric *COP* of over 20 would be achieved for the optimised solar desiccant cooling system in Australia, which also provides some reliability for the simulation results and contributes to the system model validation. In addition, the annual averaged system *COP* increases from 10.0 for 10 m^3 storage tank volume to about 13.2 for 50 m^3 storage tank volume.

Figure 8 below demonstrates the influence of the storage tank volume on the annual backup heater energy consumption. The figure shows that increasing the storage tank volume will decrease the backup heater energy consumption. When enlarging the storage tank volume from 10 to 20 m^3, the annual backup heater energy consumption will reduce about 39 GJ from 193 to 154 GJ. However, the backup heater energy consumption reduction is not in proportion with the storage tank volume increment. For every 10 m^3 of storage tank volume increment, the backup heater energy savings decreases with the tank volume increases. In other words, the larger the storage tank volume is, the smaller the amount of backup heater energy savings can be achieved. For instance, when raising the tank volume from 40 to 50 m^3, only about 9 GJ backup heater energy can be saved. Therefore, it is not recommended to increase the storage tank volume immoderately if considering the storage tank investment cost.

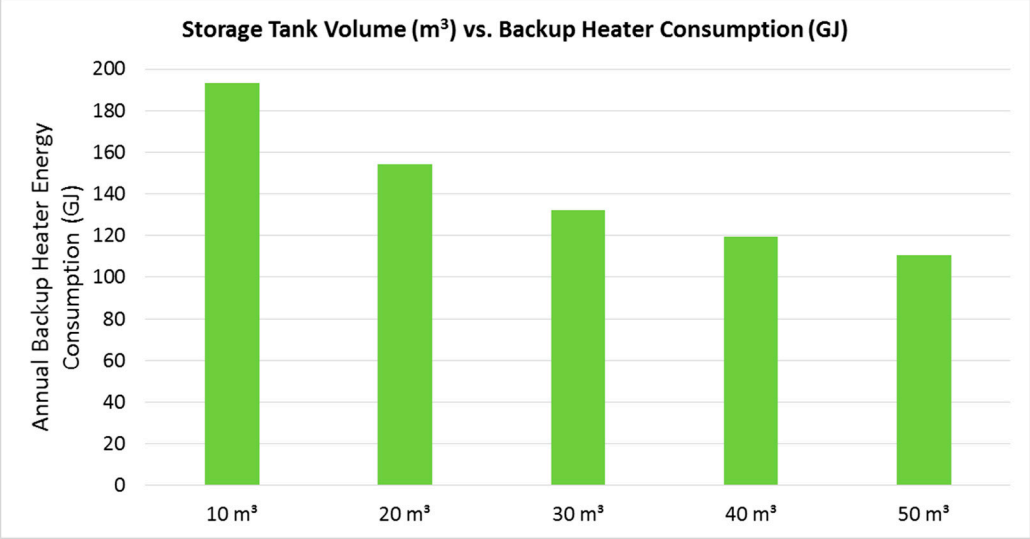

Figure 8. The impact of storage tank volume on backup heater energy consumption.

3.2. The Impacts of Solar Collector Area

According to Henning [34], a typical value of the suggested solar collector area for a solar cooling system is about 10 m^2 per 1000 m^3/h of nominal supply air flow rate. The simulation result indicates that the design supply air flow rate of the proposed SDEC system for this typical office building in Brisbane is about 16 m^3/s. Therefore, the selected values for the solar collector areas vary from 576 m^2 to 684 m^2 with interval 36, representing the supply air volume of 16 m^3/s, 17 m^3/s, 18 m^3/s, and 19 m^3/s respectively. For the hydraulic connection of the solar array, it assumes that the solar array is consisted of 32 to 38 rows in parallel, with each row of about 18 m^2 collector area, mounted on the

roof of the building. This means that nine solar collector modules are in series in each row, as each module is 1.98 m^2 for the selected Solarhart Industries Bt solar thermal collector. The impacts of the solar collector area on system *SF*, *COP* and annual backup heater energy consumption are shown in Figures 9–11 below. This result analysis is based on the fixed storage tank volume of 40 m^3 and backup heater capacity of 100 kW.

Figure 9 implies that the monthly *SF* rises with the increase of the solar collector area. When improving the installed solar collector area from 576 to 684 m^2, the average annual *SF* could boost from 0.768 to 0.798. This is because the larger the solar collector area, the more energy gains from the sun. It is also noted that in winter seasons from April to August and in some summer periods like November and December, the SF increment is more obvious than in other months. This is because in these months, the useful solar energy Q_{Solar} increases apparently with the enlargement of the collector area. While in summer seasons from January to March, since the solar energy gain is relatively high enough, increasing the solar collector area will not apparently increase the useful solar utilisation.

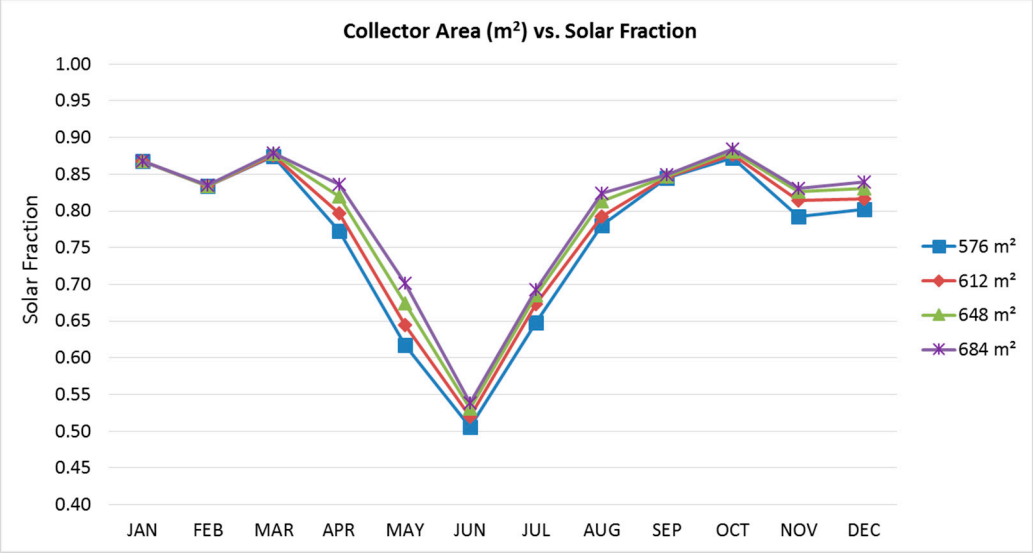

Figure 9. The impact of the solar collector area on solar fraction.

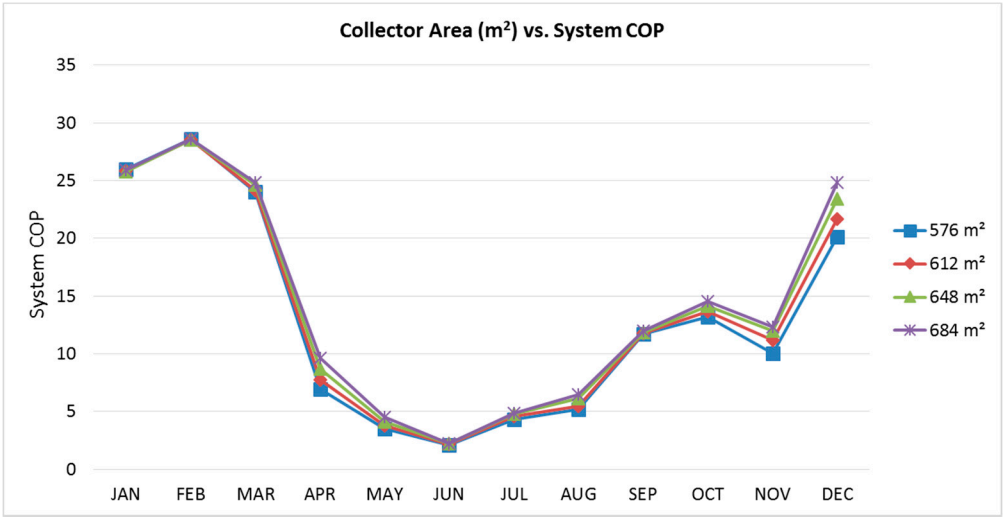

Figure 10. The impact of the solar collector area on system COP.

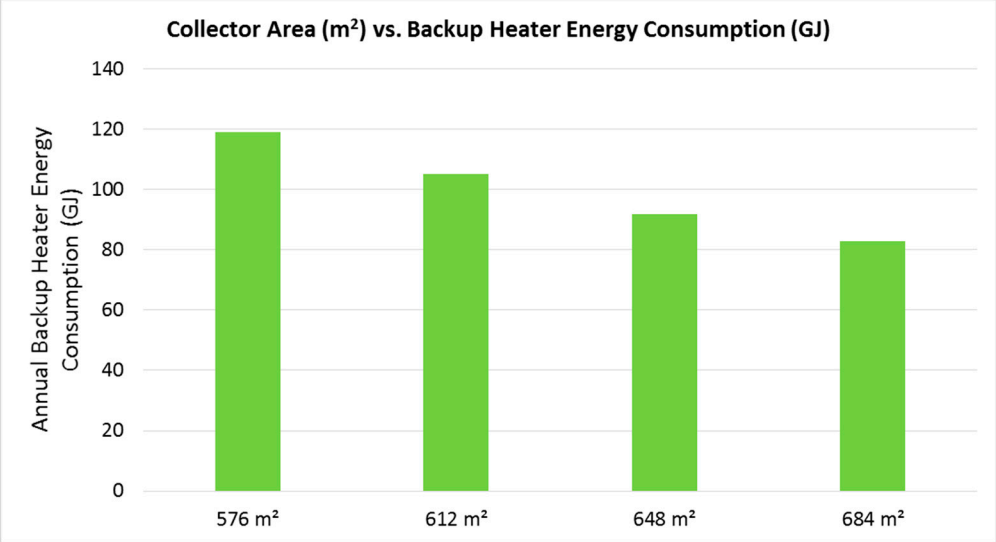

Figure 11. The impact of the solar collector area on annual backup heater energy consumption.

Figure 10 shows the impact of the solar collector area on system *COP*. It indicates that the system *COP* increases slightly with the growth of the solar collector area, because it results in a reduced total HVAC electrical power consumption, especially for the backup heater. However, the increment is not quite as dramatic as that compared with the impact of changing storage tank volume.

Figure 11 illustrates the relation of the backup heater energy consumption with the solar collector area. It shows that the backup heater energy consumption decreases as the collector area increases. When changing the collector area from 576 to 612 m^2, the backup heater could save 14 GJ electricity energy annually from 119 to 105 GJ. However, when the collector area continues to increase, the backup heater energy savings become smaller, which are about 13 GJ from 612 to 648 m^2, and 9 GJ from 648 to 684 m^2. In addition, the energy savings effect of increasing the solar collector area is not as dramatic as the effect of increasing the storage tank volume.

3.3. The Impacts of Backup Heater Capacity

The backup heater is an important auxiliary component for the solar air conditioning system which is used to provide supplementary thermal power when solar energy is insufficient. The capacity of the backup heater is a key element to the system performance in terms of the backup heater energy consumption and the backup heater hot water outlet set-point temperature. In order to assess the influence of the backup heater capacity on the system performance, four variables of the backup heater capacity were evaluated: 50, 100, 200 and 300 kW. The maximum of 300 kW was selected based on the assumption that no solar thermal energy is contributed to the system and all thermal heat required for regeneration comes from the backup heater. The backup heater energy consumption and the entering regeneration heating coil hot water temperature are the two performance indicators. The backup heater capacity analysis is based on the fixed storage tank volume of 40 m^3 and collector area of 576 m^2.

Figure 12 demonstrates the monthly backup heater energy consumption with various backup heater capacities. The figure indicates that the backup heater consumes more energy in winter from April to August. This is because of low solar energy gains in winter, while at the same time dehumidifying the outdoor air is still required in Brisbane. The backup heater also consumes substantial electricity in November. This is due to high dehumidification demand in November. In addition, the 50 kW heater capacity requires the least annual total electrical energy, while the backup heater consumes the most annual electricity when the capacity is 100 kW. However, the backup heater's energy consumption is quite similar between 100, 200 and 300 kW capacity.

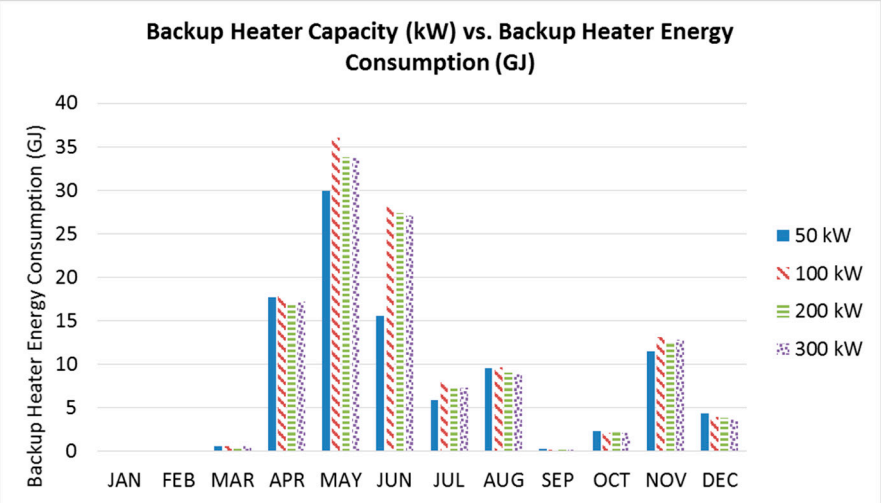

Figure 12. The impact of backup heater capacity on backup heater energy consumption.

Figure 13 shows the impact of backup heater capacity on the regenerative heating coil inlet water temperature $T_{reg,w,in}$. The figure illustrates that in cooling and dehumidification dominated months from August to December and from January to April, the regeneration heating coil hot water inlet temperature can meet the design set-point of 75 °C with 5 °C dead band for all capacities. In winter months from May to July, the 50 kW heater capacity could not satisfy the design set-point temperature for the regeneration heating coil hot water inlet due to insufficient heater capacity. However, for the other three heater capacities, the monthly $T_{reg,w,in}$ is quite similar, all above 72 °C.

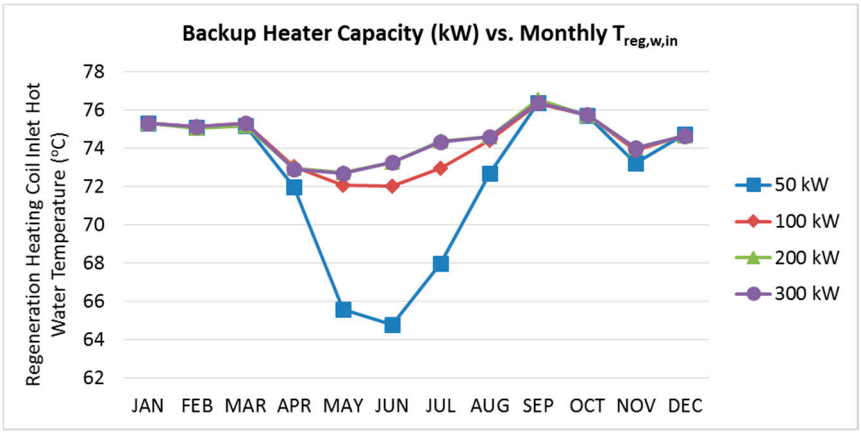

Figure 13. The impact of backup heater capacity on $T_{reg,w,in}$.

Figure 14 clearly demonstrates the impact of varying backup heater capacities on the annual backup heater energy consumption and the yearly average regeneration heating coil hot water inlet temperature. The figure implies that although 50 kW heater capacity consumes the least backup electricity of only 97.65 GJ annually, the regeneration heating coil hot water inlet temperature could not reach its set-point on the yearly average, which will definitely lower the dehumidifying effect, especially in winter months when dehumidification is still required. This is because in Brisbane, the outdoor humidity ratio in some winter periods is still above the dehumidification trigger set-point of 0.008 kg/kg. Since the 100 kW heater capacity has quite similar performances with bigger capacities on the annual E_{Aux} and the yearly averaged $T_{reg,w,in}$, considering the backup heater investment cost factor, 100 kW backup heater capacity would probably be the best choice for this system.

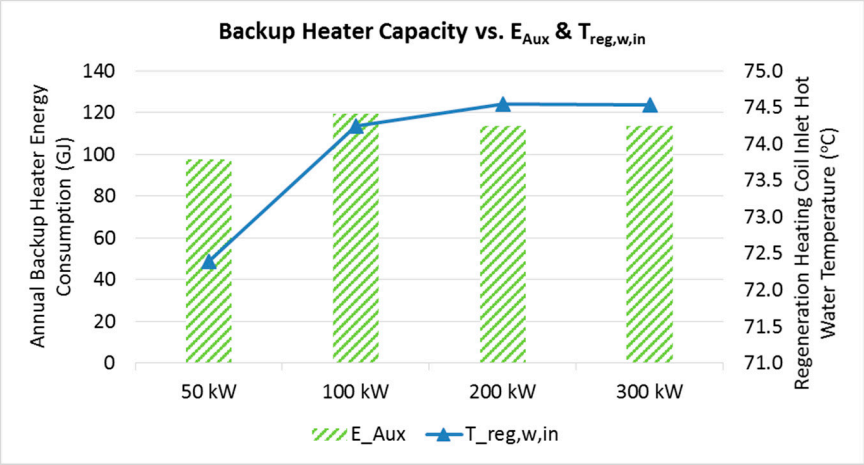

Figure 14. The impact of varying backup heater capacity on E_{Aux} and $T_{reg,w,in}$.

3.4. Economic Optimization of Storage Tank Volume and Solar Collector Area

From the above discussion in Sections 3.1 and 3.2, it is concluded that either increasing the storage tank volume or increasing the solar collector area could lead to increased system *SF* and system *COP* while at the same time decrease the backup heater electricity energy consumption. As the storage tank volume and solar collector area are two important parameters that influence the solar desiccant cooling system performance, it is crucial to investigate their impacts as a whole. In addition, considering the investment cost, it is also significantly important to evaluate the optimized storage tank volume and solar collector area configuration from the economic point of view for the SDEC system. Therefore, a *LCC* analysis for the solar subsystem is also conducted. Figure 15 below illustrates how the storage tank volume and solar collector area together influence the system backup heater energy consumption. The simulations are based on 100 kW backup heater capacity.

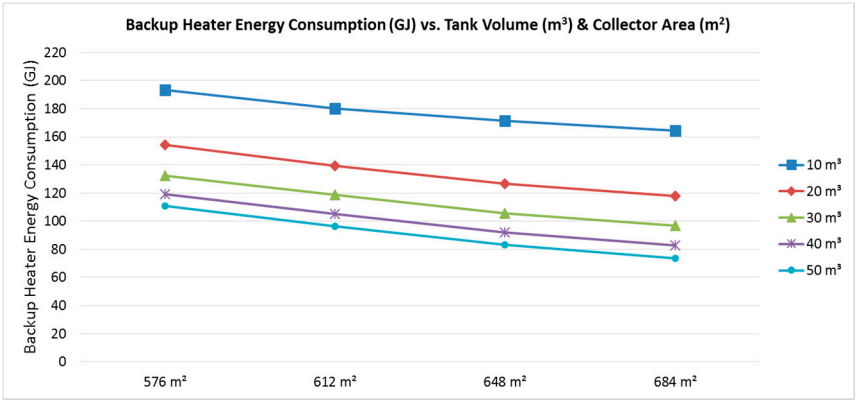

Figure 15. The impacts of tank volume and collector area on annual backup heater energy consumption.

From the figure it is clear that the backup heater energy consumption decreases with the increase of the storage tank volume and solar collector area. In addition, increasing the storage tank volume would result in more backup heater energy conservation than increasing the solar collector area. It points out that boosting the storage tank volume from 10 to 50 m^3 would achieve about 83 GJ annual backup heater energy savings while only less than 40 GJ backup heater energy could be saved by increasing the solar collector area from 576 to 684 m^2. Therefore, increasing the storage tank volume would contribute to more energy savings than improving the solar collector area. However,

with the increment of the storage tank volume, the backup heater energy savings potential becomes less obvious.

Figure 16 demonstrates the life cycle cost of different storage tank volume and solar collector area configurations for the solar subsystem of the SDEC system. The inflation rate is selected as 2.5% [22]. The discount rate is 8% and system lifespan is assumed as 25 years [1]. The commercial electricity fuel cost in Brisbane is 10.48 c/kWh [3]. The maintenance cost is assumed to be 1% of the total investment cost of the solar subsystem [26]. All other economic assumptions including the initial cost of the solar collector, storage tank, backup heater, and solar water pumps are referenced from [35]. The economic parameters for the *LCC* calculation are summarized in Table 5.

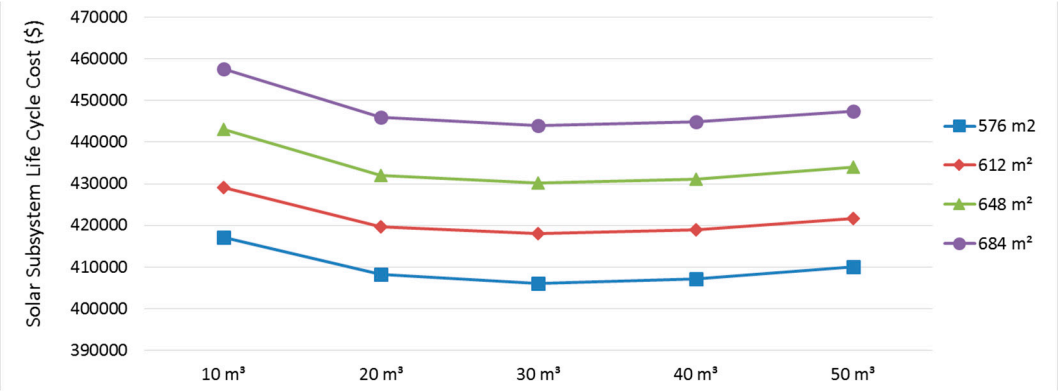

Figure 16. Solar subsystem *LCC* vs. storage tank volume and collector area.

Table 5. Cost of different components and economic parameters [35].

Components	Value
Solar collector	423 \$/m^2
Storage tank	550 \$/m^3
Backup heater	440 \$/kW
Solar water pumps	\$8840
Electricity fuel cost	10.48 c/kWh
System lifespan	25 years
Inflation rate	2.5%
Discount rate	8%

The *LCC* is calculated using the present value method by introducing a present worth factor (*PWF*), which is used to compare the future cost of a product to today's cost taken into account an obligation recurs each year at i inflation rate and d discount rate over N years of lifespan [36]. The *LCC* is then calculated by the following equations [36,37]:

$$PWF(N,\ i,\ d) = \sum_{j=1}^{N} \frac{(1+i)^{j-1}}{(1+d)^{j}} = \begin{cases} \frac{1}{d-i}\left[1-\left(\frac{1+i}{1+d}\right)^{N}\right],\ if\ i \neq d \\ \frac{N}{i+1},\ if\ i = d \end{cases} \quad (13)$$

$$LCC = IC + PWF \times OC \quad (14)$$

where *PWF* implies the present worth factor; i is the inflation rate; d is the discount rate; N is the lifetime of the system; *IC* is the total initial investment cost of the solar subsystem; and *OC* is the annual operating cost which consists of the annual fuel cost and maintenance cost.

The *LCC* results indicate that the 576 m^2 solar collector configuration has the lowest solar subsystem *LCC* regardless of the storage tank volume. The larger the solar collector area, the higher the *LCC*. It also indicates that 30 m^3 storage tank volume configuration has the lowest *LCC* for all solar

collector area configurations. The lowest *LCC* happens in 30 m^3/576 m^2 storage capacity configuration with $405,954.

3.5. The Impacts of Outdoor Air Humidity Ratio Control

The outdoor air humidity ratio control strategy applied to the SDEC system controls the operation of the desiccant dehumidification process. It aims at reducing unnecessary regeneration energy consumption when dehumidifying is not required. It is accomplished by an actuator on the EMS that senses the outdoor air humidity ratio. Therefore, to analyse its impact on the SDEC system performance, four outdoor air humidity ratio control set-point values have been assessed, which are 0.006, 0.008, 0.010 and 0.012 kgWater/kgDryAir. The backup heater energy consumption and indoor thermal conditions are the indicators as illustrated in Figure 17 below. The analysis is based on 576 m^2 collector area, 40 m^3 storage tank volume, and 100 kW backup heater capacity. The Time Set-point Not Met During Occupied Cooling means the ratio of the unmet indoor cooling set-point hours to the total HVAC operation hours in a year (3120 h of HVAC operation).

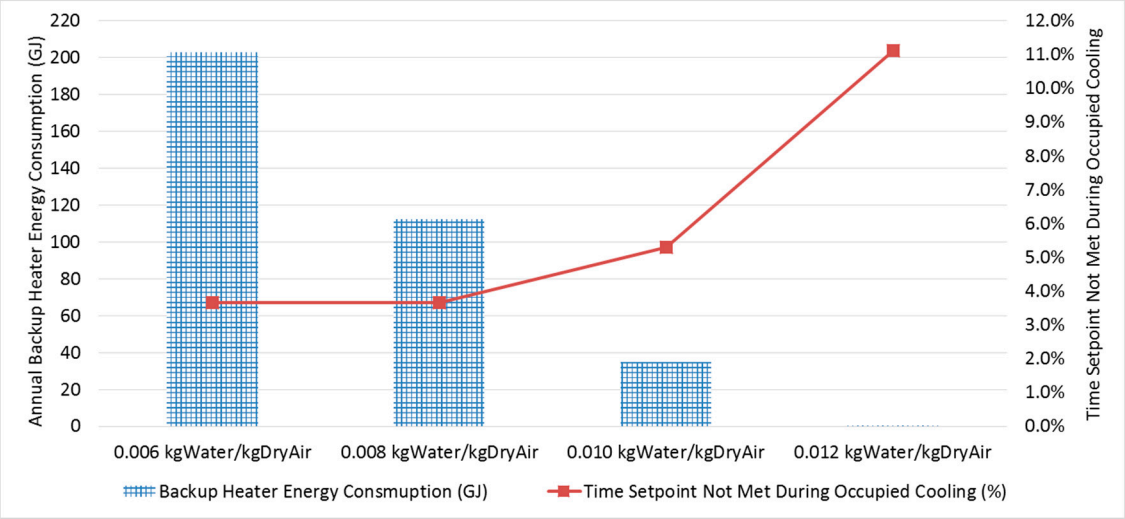

Figure 17. The impact of the outdoor air humidity ratio control on backup heater energy consumption and indoor thermal conditions.

It shows that the higher the outdoor air humidity ratio set-point is, the lower the backup heater electricity consumption is. When increasing the outdoor air humidity ratio control set-point from 0.006 to 0.012 kgWater/kgDryAir, the annual backup heater energy consumption reduces dramatically from 203 to about 0.33 GJ. This is because of the reduced desiccant dehumidifying operation when improving the outdoor air humidity ratio actuator set-point.

However, this will increase the frequency of high indoor temperature events. The indoor cooling set-point unmet time could increase significantly from 3.7 to 11.1% when increasing the outdoor air humidity ratio control set-point from 0.006 to 0.012 kgWater/kgDryAir. It is quite obvious that when the outdoor air humidity ratio control set-point goes above 0.008 kg/kg, the unmet indoor cooling set-point time soars exponentially. While decreasing the outdoor air humidity ratio control set-point below 0.008 kgWater/kgDryAir would not impact the indoor thermal condition but increase the backup heater energy consumption dramatically. Therefore, the 0.008 kgWater/kgDryAir outdoor air humidity control set-point seems to be the most reasonable value for this SDEC system under Brisbane climate.

4. Conclusions

This paper has evaluated the factors that influence the SDEC system performance for a typical office building in Brisbane, Australia, in terms of the storage tank volume, solar collector area, backup heater capacity, and outdoor air humidity control set-point. The sensitivity analysis results have indicated that either increasing the storage tank volume or increasing solar collector area could result in improved system *SF* and system *COP*, while at the same time reduce backup heater energy consumption. When increasing the storage tank volume from 10 to 50 m^3, the annual average system *SF* was increased by 11.4% from 0.7 to 0.78, and the annual average system electric *COP* was increased by 32% from 10.0 to 13.2. Meanwhile, the annual backup heater energy consumption was reduced by 43% from about 193 to 110 GJ.

On the other hand, increasing the installed solar thermal collector area from 576 to 684 m^2 resulted in 3.9% increase in the annual average system *SF* and 23% increase in the annual average system electric *COP*, along with about 30.4% annual backup heater energy savings. These implied that the storage tank volume was more sensitive to the SDEC system energy performance than the solar collector area. In addition, from the economic point of view, the 30 m^3/576 m^2 storage tank volume to solar collector area ratio has the lowest solar subsystem *LCC* of $405,954, which was the optimized configuration relating to storage tank volume and solar collector area.

In relation to the backup heater capacity, 100 kW heater capacity appeared to be preferable, which could satisfy the 75 °C design regeneration heating coil hot water inlet temperature set-point with relatively low backup heater electricity consumption of 119 GJ annually. However, more than 100 kW backup heater capacity would not apparently influence the regeneration heating coil hot water inlet temperature and the backup heater energy consumption.

Finally, increasing the outdoor air humidity ratio actuator set-point for dehumidification control would dramatically reduce backup heater energy consumption perhaps at the expense of indoor thermal conditions. An outdoor air humidity ratio control set-point of 0.008 kgWater/kgDryAir was more reasonable, which could achieve both low backup heater energy consumption and good indoor thermal conditions with only 3.7% time set-point not met during occupied cooling.

Acknowledgments: The authors would like to acknowledge that Queensland University of Technology (QUT) provided the funds for covering the costs to publish in open access.

Author Contributions: Yunlong Ma and Lisa Guan conceived the project. Yunlong Ma created the building and system model, and conducted the simulation. Yunlong Ma, Lisa Guan and Wendy Miller analyzed and presented the simulation results data. Yunlong Ma wrote the paper. Suvash C. Saha and Wendy Miller provided revisions and feedback for the paper manuscript. Suvash C. Saha applied for the funds for open access publication.

Conflicts of Interest: The authors declare no conflict of interest.

Nomenclature

A_c	Solar collector area (m^2)
B_{1-8}	Temperature equation coefficients for the desiccant wheel
C_{1-8}	Humidity ratio equation coefficients for the desiccant wheel
COP	Coefficient of performance
C_w	Specific heat of the collector working fluid (kJ/kg/K)
c_0	Solar thermal collector optical efficiency
c_1, c_2	Solar thermal collector heat loss coefficients ($W/m^2 \cdot K$ and $W/m^2 \cdot K^2$)
d	Discount rate (%)
E_{Aux}	Electricity energy consumption by the backup heater (GJ)
E_{Solar}	Useful solar thermal energy input for regeneration (GJ)
E_{in}	Total energy input for driving the solar desiccant cooling system (GJ)
E_{hvac}	Energy input of fans, pumps, backup heater, desiccant wheel, and evaporative coolers (GJ)
h_o	Enthalpy of outside air (kJ/kg)
h_s	Enthalpy of supply air (kJ/kg)

h·A	The air-to-air heat exchanger surface convective heat transfer coefficient multiply by the heat exchanger heat transfer area (W)
I	Total incident solar radiation (W/m^2)
i	Inflation rate (%)
IC	Total initial investment cost of the solar subsystem ($)
m_o	Outside air mass flow rate (kg/s)
m	Mass flow rate of the working fluid through the collector (kg/s)
N	Lifespan of the system
OC	Annual operating cost of the solar subsystem ($)
PTI	Process inlet air dry bulb temperature (°C)
PWI	Process inlet air humidity ratio (kg/kg)
PWF	Present worth factor
Q_C	System cooling effect (kW)
Q_{Solar}	Solar energy gains from solar thermal collectors (kW)
RFV	Regeneration (and process) air face velocity (m/s)
RWI	Regeneration inlet air humidity ratio (kg/kg)
RWO	Regeneration outlet air humidity ratio (kg/kg)
RTI	Regeneration inlet air dry bulb temperature (°C)
RTO	Regeneration outlet air dry bulb temperature (°C)
SF	Solar fraction
t_{1-9}	Dry bulb temperature of the air at each point in Figure 1 (°C)
w_{1-9}	Humidity ratio of the air at each point in Figure 1 (kgWater/kgDryAir)
T_a	Ambient air temperature (°C)
$T_{db,in}$	Evaporative cooler inlet air dry bulb temperature (°C)
$T_{db,out}$	Evaporative cooler outlet air dry bulb temperature (°C)
T_{in}	Water inlet temperature of the solar collector and backup heater (°C)
T_{set}	Hot water set-point temperature in the backup heater (°C)
$T_{reg,w,in}$	Regenerative heating coil inlet water temperature (°C)
$\overline{T}$	Mean temperature of T_{in} and T_{set} (°C)
$T_{wb,in}$	Evaporative cooler inlet air wet bulb temperature (°C)
U_A	Overall heat loss coefficient of the backup heater to environment during operation (W/m^2·K)
W_{in}	Total energy input for driving the HVAC system (kW)
W_{hvac}	Electricity power input of all the HVAC electric components (kW)
ε	Direct evaporative cooler effectiveness
ε_{HX}	Air-to-air heat exchanger effectiveness
η_{Solar}	Solar thermal collector's efficiency
η	Backup heater efficiency

References

1. Baniyounes, A.M.; Liu, G.; Rasul, M.G.; Khan, M.M.K. Analysis of solar desiccant cooling system for an institutional building in subtropical Queensland, Australia. *Renew. Sustain. Energy Rev.* **2012**, *16*, 6423–6431. [CrossRef]
2. Angrisani, G.; Roselli, C.; Sasso, M.; Tariello, F. Assessment of energy, environmental and economic performance of a solar desiccant cooling system with different collector types. *Energies* **2014**, *2014*, 6741–6764. [CrossRef]
3. Ma, Y.; Guan, L.; Brown, R. Techno-economic analysis of a solar desiccant-evaporative cooling system with different collector types for australian office buildings. In Proceedings of the Asia Pacific Solar Research Conference, Brisbane, Australia, 8–10 December 2015; Egan, R., Passey, R., Eds.; Australian PV Institute: Brisbane, Australia, 2015.
4. Rafique, M.; Rehman, S.; Lashin, A.; Al Arifi, N. Analysis of a solar cooling system for climatic conditions of five different cities of Saudi Arabia. *Energies* **2016**, *9*, 75. [CrossRef]

5. Angrisani, G.; Roselli, C.; Sasso, M.; Tariello, F.; Vanoli, G. Performance assessment of a solar-assisted desiccant-based air handling unit considering different scenarios. *Energies* **2016**, *9*, 724. [CrossRef]
6. Li, H.; Dai, Y.J.; Li, Y.; La, D.; Wang, R.Z. Case study of a two-stage rotary desiccant cooling/heating system driven by evacuated glass tube solar air collectors. *Energy Build.* **2012**, *47*, 107–112. [CrossRef]
7. Ge, T.S.; Ziegler, F.; Wang, R.Z.; Wang, H. Performance comparison between a solar driven rotary desiccant cooling system and conventional vapor compression system (performance study of desiccant cooling). *Appl. Therm. Eng.* **2010**, *30*, 724–731. [CrossRef]
8. Goldsworthy, M.; White, S. Optimisation of a desiccant cooling system design with indirect evaporative cooler. *Int. J. Refrig.* **2011**, *34*, 148–158. [CrossRef]
9. Henning, H.-M.; Motta, M.; Mugnier, D. *Solar Cooling Handbook: A Guide to Solar Assisted Cooling and Dehumidification Processes*, 3rd ed.; AMBRA: Vienna, Austria, 2013.
10. White, S.D.; Kohlenbach, P.; Bongs, C. Indoor temperature variations resulting from solar desiccant cooling in a building without thermal backup. *Int. J. Refrig.* **2009**, *32*, 695–704. [CrossRef]
11. Parmar, H.; Hindoliya, D.A. Performance of solid desiccant-based evaporative cooling system under the climatic zones of India. *Int. J. Low-Carbon Technol.* **2012**, *8*, 52–57. [CrossRef]
12. Hatami, Z.; Saidi, M.H.; Mohammadian, M.; Aghanajafi, C. Optimization of solar collector surface in solar desiccant wheel cycle. *Energy Build.* **2012**, *45*, 197–201. [CrossRef]
13. Panaras, G.; Mathioulakis, E.; Belessiotis, V. Solid desiccant air-conditioning systems—Design parameters. *Energy* **2011**, *36*, 2399–2406. [CrossRef]
14. Rafique, M.; Rehman, S.; Alhems, L.; Lashin, A. Parametric analysis of a rotary type liquid desiccant air conditioning system. *Energies* **2016**, *9*, 305. [CrossRef]
15. Santori, G.; Sapienza, A.; Freni, A. A dynamic multi-level model for adsorptive solar cooling. *Renew. Energy* **2012**, *43*, 301–312. [CrossRef]
16. ABCB. *ABCB Energy Modelling of Office Buildings for Climate Zoning (Class 5 Climate Zoning Consultancy) Stages 1, 2 & 3*; Australian Building Codes Board: Canberra, Australia; ACADS-BSG: Glen Iris, Australia, 2002.
17. ABCB. *ABCB Energy Modelling of Office Buildings for Climate Zoning (Class 5 Climate Zoning Consultancy) Stages 4 & 5*; Australian Building Codes Board: Canberra, Australia; ACADS-BSG: Glen Iris, Australia, 2002.
18. Daly, D.; Cooper, P.; Ma, Z. Understanding the risks and uncertainties introduced by common assumptions in energy simulations for Australian commercial buildings. *Energy Build.* **2014**, *75*, 382–393. [CrossRef]
19. Daly, D.; Cooper, P.; Ma, Z. Implications of global warming for commercial building retrofitting in Australian cities. *Build. Environ.* **2014**, *74*, 86–95. [CrossRef]
20. Ma, Y.; Guan, L. Performance analysis of solar desiccant-evaporative cooling for a commercial building under different Australian climates. In Proceedings of the 9th International Symposium on Heating, Ventilation and Air Conditioning (ISHVAC)—The 3rd International Conference on Building Energy and Environment (COBEE), Tianjin, China, 12–15 July 2015; Sun, Y., Pei, J., Eds.; Procedia Engineering: Tianjin, China, 2015; Volume 121, pp. 528–535.
21. Bannister, P. *Australian Building Codes Board: Class 5 Benchmarking*; Exergy Australia Pty Limited: Belconnen, Australia, 2004.
22. Donnelly, E. *Economic Analysis of Energy Provisions for Base Building Fabric Elements of Air-Conditioned Office Spaces*; Australian Building Codes Board: Canberra, Australia, 2004.
23. ABCB. *National Construction Code 2016 Building Code of Australia—Volume One*; The Australian Building Codes Board: Canberra, Australia, 2016.
24. Egan, A.M. Air tightness of Australian offices buildings: Reality versus typical assumptions used in energy performance simulation. In Proceedings of the 12th Conference of International Building Performance Simulation Association, Sydney, Australia, 14–16 November 2011.
25. Feng, X.; Yan, D.; Peng, C.; Jiang, Y. Influence of residential building air tightness on energy consumption. *HVAC* **2014**, *44*, 5–14.
26. Henning, H.-M. *Solar-Assisted Air-Conditioning in Buildings*, 2nd ed.; SpringerWienNewYork: Stefan, Austria, 2007.
27. Selke, T.; Frein, A. *Collection of Good Practices for DEC Design and Installation*; IEA Solar Heating and Cooling Program: 2015, Task 48—Activity B2 Final Report, November 2015; Daniel Mugnier: Perpignan, France; Available online: http://task48.iea-shc.org/publications (accessed on 4 May 2017).

28. SOLAVIS. Flat Plate Collectors v Evacuated Tubes—A Brief Overview. 2008. Available online: www.solarvis.com.au (accessed on 4 May 2017).
29. DOE. EnergyPlus Engineering Reference. Available online: https://energyplus.net/documentation (accessed on 5 January 2016).
30. Desiccant Rotors International Pvt. Ltd. Technical Specification of ECO-DRY Desiccant Cassette. Available online: http://www.drirotors.com/ (accessed on 17 September 2015).
31. Dezfouli, M.M.S.; Mat, S.; Pirasteh, G.; Sahari, K.S.M.; Sopian, K.; Ruslan, M.H. Simulation analysis of the four configurations of solar desiccant cooling system using evaporative cooling in tropical weather in Malaysia. *Int. J. Photoenergy* **2014**, *2014*, 1–14. [CrossRef]
32. Baniyounes, A.M.; Liu, G.; Rasul, M.G.; Khan, M.M.K. Comparison study of solar cooling technologies for an institutional building in subtropical Queensland, Australia. *Renew. Sustain. Energy Rev.* **2013**, *23*, 421–430. [CrossRef]
33. Guangzhou Jiema Heat Exchange Equipment Co., Ltd. Air to Air Heat Exchanger. Available online: www.jiema-heatexchangers.com (accessed on 5 January 2016).
34. Henning, H.-M. Solar assisted air conditioning of buildings—An overview. *Appl. Therm. Eng.* **2007**, *27*, 1734–1749. [CrossRef]
35. Ma, Y. Investigation of Advanced Solar-assisted Cooling for Australian Commercial Buildings. Master' Thesis, Queensland University of Technology, Brisbane, Australia, 2016.
36. Duffie, J.A.; Beckman, W.A. *Solar Engineering of Thermal Processes.*, 4th ed.; John Wiley & Sons, Inc.: Hoboken, NJ, USA, 2013.
37. Abdel-Salam, A.H.; Ge, G.; Simonson, C.J. Thermo-economic performance of a solar membrane liquid desiccant air conditioning system. *Sol. Energy* **2014**, *102*, 56–73. [CrossRef]